International Journal of Bifurcation and Chaos, Vol. 32, No. 6 (2022) 2250078 (14 pages)

DOI: 10.1142/S021812742250078X

Fractal Structures and Magnetic Footprints in a Divertor Tokamak

A. C. Mathias, G. Perotto and R. L. Viana
Department of Physics, Federal University of Paraná, 81531-990 Curitiba, Paraná, Brazil

A. Schelin
Institute of Physics, University of Brasília, 70910-900 Brasília, Distrito Federal, Brazil

I. L. Caldas
Institute of Physics, University of São Paulo, 05315-970 São Paulo, São Paulo, Brazil

Received ; Revised

Fractal structures appear very often in open Hamiltonian systems, and can be identified in the deposition of chaotic magnetic field line on the plates of a tokamak divertor. Indeed, tokamaks with divertors are used to control the magnetic confinement of plasmas, such that the field lines created by electric currents have escape channels, through which plasma particles can be diverted out of the tokamak wall and redirected to divertor plates. In this work, we use a symplectic map to investigate the deposition patterns on the plates of a divertor. We show that the pattern of magnetic footprints on divertor plates (deposition patterns) underlying the chaotic orbits involves a number of fractal structures related to the existence of a nonattractive invariant chaotic set. In order to investigate the fractal characteristic of magnetic footprints, we analyze quantitatively the degree of stability of the fractal structure by calculating the entropy of the basin. These numerical analyses indicate that the fractal pattern on the divertor plates depends sensibly on the magnetic field structure. We show qualitative evidences of the Wada property.

Keywords: Fractal structure; magnetic footprint; tokamak divertor.

1. Introduction

The achievement of fusion plasma energy is a long-term goal of a number of large undertakings throughout the world, the foremost example being the ITER (International Thermonuclear Experimental Reactor), currently being assembled [Horton & Benkadda, 2015]. ITER is designed to produce a deuterium-tritium plasma in which the fusion reactions are sustained through internal heating. It is expected that, from a 50 MW of input heating power, ITER will produce 500 MW of fusion power: a ten-fold increase [Agency, 2002].

One of the major technical problems of generating a fusion plasma capable of delivering such power is the release of high-energy fusion products such as Helium atoms or impurity atoms created from plasma-wall interactions [Post & Behrisch, 1986]. The resulting heat and particle transport in ITER is expected to generate heat loads of 5–10 $\mathrm{MW/m^2}$ that can damage the tokamak inner wall [Federici *et al.*, 2003].

In order to mitigate this undesirable effect, the concept of a divertor has been developed, which is a shaped metallic plate placed outside the plasma

boundary so as to capture or divert particles escaping from the plasma [Cordey *et al.*, 1992]. Besides ITER, other currently operating tokamak devices like JET (Joint European Torus) and Alcator C-Mod also use divertors with this purpose [Bertolini *et al.*, 1992; Lipschultz *et al.*, 2007].

The basic idea underlying the operation of a divertor is that magnetic field lines can be arranged so as to deviate charged particles from the outer plasma region and direct them to a metallic plate. However, if the heat and particle loadings are not mitigated, the divertor plates could be damaged as well. In order to do so, a chaotic region of magnetic field lines in the outer plasma region is created. This helps to distribute such loadings over a larger region of the plates, forming the so-called *magnetic footprints*.

It was experimentally observed that magnetic footprints in divertor plates are not uniform, and show a degree of self-similar behavior [Kroetz *et al.*, 2008; Jakubowski *et al.*, 2009]. In other words, the points comprising the magnetic footprints correspond to chaotic trajectories that spend widely different times before escaping to the divertor plates. Hence the of hot spots (particles with large escape times) and cold spots (small escape times) in a magnetic footprint are mixed together in a complicated fashion. The particles with a long escape time can come from inner regions of the chaotic layer and reach the divertor plate carrying energetic particles from the inside of the plasma, hence the name hot spots.

The main point of the present paper is that magnetic footprints is a kind of fractal structure which ultimately arises from the nonintegrable nature of the magnetic field line structure [da Silva *et al.*, 2002]. The structure of invariant manifolds act as escape channels through which plasma particles are directed to the divertor plate, forming magnetic footprints on it [Abdullaev *et al.*, 1998; Abdullaev & Finken, 1998; Abdullaev *et al.*, 1999; Abdullaev *et al.*, 2001; Portela *et al.*, 2008]. One of the tools recently developed to investigate the uncertainty inherent to such fractal structures is the so-called basin entropy [Daza *et al.*, 2016, 2017]. This is a measure of the final-state unpredictability of a dynamical system, given the fractal nature of the corresponding basins. If the system is dissipative, we analyze basins of attraction, but if is conservative, we analyze basins of escape [Aguirre *et al.*, 2001]. We investigate the relation between fractal basins of escape and magnetic footprints in a divertor tokamak using the basin entropy as the main tool.

This paper is organized as follows: in Sec. 2 we outline the basics of the magnetic field line structure in a divertor tokamak, emphasizing the Hamiltonian nature of the equations. In Sec. 3, we consider an area-preserving two-dimensional map proposed to investigate a divertor tokamak, exploring some of its dynamical properties. In Sec. 4, we present some numerical examples of escape patterns of magnetic field lines on the divertors plate. In Sec. 5, we characterize the fractality of magnetic footprints. In Sec. 6, we verify the existence of the Wada property, an extreme form of fractality. Finally, in Sec. 7, we report our conclusions.

2. Magnetic Field Line Map

The tokamak is a toroidal device for the magnetic confinement of a high-temperature plasma using two main magnetic fields: the toroidal field $\mathbf{B}_T$ created by external coils and the poloidal field $\mathbf{B}_P$, generated by the plasma itself. The equilibrium field $\mathbf{B}_0 = \mathbf{B}_T + \mathbf{B}_P$ has helical magnetic lines of force on toroidal surfaces called magnetic surfaces. The magnetic surface with zero volume is called magnetic axis. Figure 1(a) depicts the basic tokamak geometry used in this paper. We denote by R_0 the distance between the magnetic axis and the symmetry (vertical) axis, and by ϕ the toroidal angle.

If we assume that the Tokamak plasma is in a MHD equilibrium state with axial symmetry it is possible to describe magnetic field line structure by a Hamiltonian description, by considering the toroidal angle ϕ as a timelike coordinate [Whiteman, 1977; Bernardin & Tataronis, 1985]. Let (x^1, x^2, x^3) denote the contravariant coordinates and $\mathbf{B} = (B^1, B^2, B^3)$ the contravariant magnetic field components. The canonical variables are $q = x^1$,

$$p = \int dx^2 \sqrt{g} B^3(x^1, x^2) + \gamma(x^1, x^3), \qquad (1)$$

where $g = \det g_{ij}$ is the determinant of the covariant metric tensor, and we consider the ignorable coordinate $t = x^3$ as the timelike variable.

The magnetic field line equations, viz. $\mathbf{B} \times \mathbf{d}\boldsymbol{\ell} = \mathbf{0}$, where $\mathbf{d}\boldsymbol{\ell}$ is the line element along the field line, can be written as Hamilton's equations

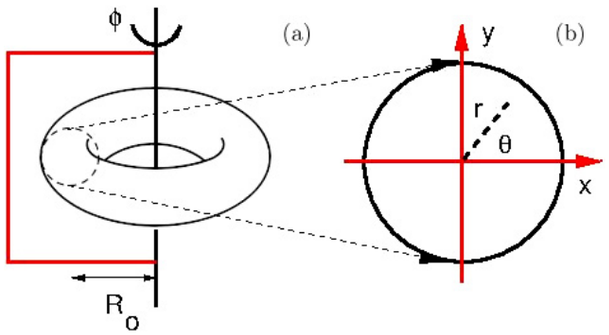

Fig. 1. (a) Schematic figure showing the basic geometrical features of a Tokamak and (b) field line coordinates in a Poincaré surface of section $\phi = 0$.

of motion

$$\frac{dq}{dt} = \frac{\partial H}{\partial p}, \quad \frac{dp}{dt} = -\frac{\partial H}{\partial q}. \tag{2}$$

The variables (q, p) are the canonical coordinates of position and moment, respectively, and t is the canonical time. The field line Hamiltonian is given by

$$H = \int dx^2 \sqrt{g} B^1(x^1, x^2) + \delta(x^1, x^2), \tag{3}$$

and the functions γ and δ are related to the canonical moment and the field line Hamiltonian through Eqs. (1) and (3), respectively. These functions must be chosen so as to satisfy the following identity

$$\sqrt{g} B^2 + \frac{\partial H}{\partial x^1} + \frac{\partial p}{\partial x^3} = 0. \tag{4}$$

Due to the axial symmetry of the overall configuration, we can study the magnetic field line structure using a Poincaré surface of section, which is a plane ($\phi = 0$). The magnetic field line position in this plane can be described by polar coordinates (x, y), where the origin is placed at the magnetic axis position [Fig. 1(b)].

The polar coordinates of the n-th intersection of a given magnetic field line with the surface section at $\phi = 0$ are denoted (x_n, y_n). A Poincaré map relates the coordinates of two consecutive intersections of a field line with this plane, namely

$$x_{n+1} = F(x_n, y_n), \tag{5}$$

$$y_{n+1} = G(x_n, y_n), \tag{6}$$

where the functions (F, G) depend on the field line Hamiltonian (3) and are usually obtained by integrating numerically the field line equation.

The Hamiltonian nature of the magnetic field line flow implies that the Poincaré map (5) and (6) is area-preserving in the surface section, that is,

$$\det \mathbf{J} = \begin{vmatrix} \dfrac{\partial x_{n+1}}{\partial x_n} & \dfrac{\partial x_{n+1}}{\partial y_n} \\ \dfrac{\partial y_{n+1}}{\partial x_n} & \dfrac{\partial y_{n+1}}{\partial y_n} \end{vmatrix} = 1. \tag{7}$$

According to MHD theory, equilibrium magnetic field lines lie on toroidal nested magnetic surfaces (also called flux surfaces, since the magnetic flux they enclose is constant), and form concentric circles in the surface section $\phi = 0$. The plasma boundary is a magnetic surface of radius a, which is separated from the vessel inner wall by a region often called *scrape-off layer*, where particles coming from the plasma core diffuse and eventually collide with the wall.

Using polar coordinates in the surface section (r_n, θ_n), defined as $x_n = r_n \cos\theta_n$ and $y_n = r_n \sin\theta_n$ [Fig. 1(b)] we have, in the lowest order approximation, the Poincaré map corresponding to equilibrium

$$r_{n+1} = r_n, \tag{8}$$

$$\theta_{n+1} = \theta_n + \iota(r_{n+1}), \tag{9}$$

where ι is called rotational transform. After each iteration of this map, the field line radius does not change and the poloidal angle increases from ι_n.

It is customary to write the latter as $\iota_n = 2\pi/q(r_n)$, where q is called *safety factor*, which takes on a different value for each magnetic surface. If q is a rational number of the form m/n, where m and n are coprime integers, any initial condition (r_0, θ_0) will recur after m map iterations. For q irrational any initial condition on the corresponding circle (the intersection of a torus with the surface $\phi = 0$) will densely fill the circle as n goes to infinity [Lichtenberg & Lieberman, 1992]. The tori associated with these situations are accordingly called rational and irrational, respectively. We denote by $q_{\text{axis}} = q(r = 0)$ and $q_{\text{edge}} = q(r = a)$ the corresponding values of the safety factor at the magnetic axis and the plasma edge, respectively.

Magnetic field line maps have been obtained from physical models of the equilibrium and perturbing fields. However, in many cases the explicit forms of the maps are quite complicated to deal with, specially with respect to the large number

of parameters they may contain and their possible values. Hence, sometimes it is better to work with simpler maps, with a few parameters, that allow an easier numerical investigation when these parameters are varied. Accordingly, we expect that the results of these numerical investigations can be extended to those more realistic magnetic field line maps. In the next section we consider such a field line map, in order to explore the properties of a divertor tokamak using a single parameter.

3. Field Line Map for a Divertor Tokamak

One simple configuration for a divertor tokamak consists of a horizontal metallic plate placed horizontally with respect to the plane containing the magnetic axis, and running along a limited range over the angle ϕ. Assuming that plasma particles closely follow magnetic field lines (this is only rigorously true if one neglect drifts and finite Larmor radius effects) we design magnetic field lines such that we preserve the equilibrium plasma flux surfaces, while adding magnetic field lines of the outer plasma region connected to the plasma boundary [Kroetz *et al.*, 2010].

Such a configuration is illustrated in Fig. 2(a). The plasma boundary is a separatrix with a hyperbolic point at $(x = 0, y = 1)$. Actually this design does not configure yet for a divertor tokamak, since only those field lines strictly on the separatrix could be diverted to the horizontal plate. A nonintegrable element is necessary to create a thin region of chaotic field lines near the separatrix, such that the field lines in this region (and the associated particles) are diverted to the horizontal plate. The chaotic field lines around the separatrix are created due to the symmetry breaking in the presence of

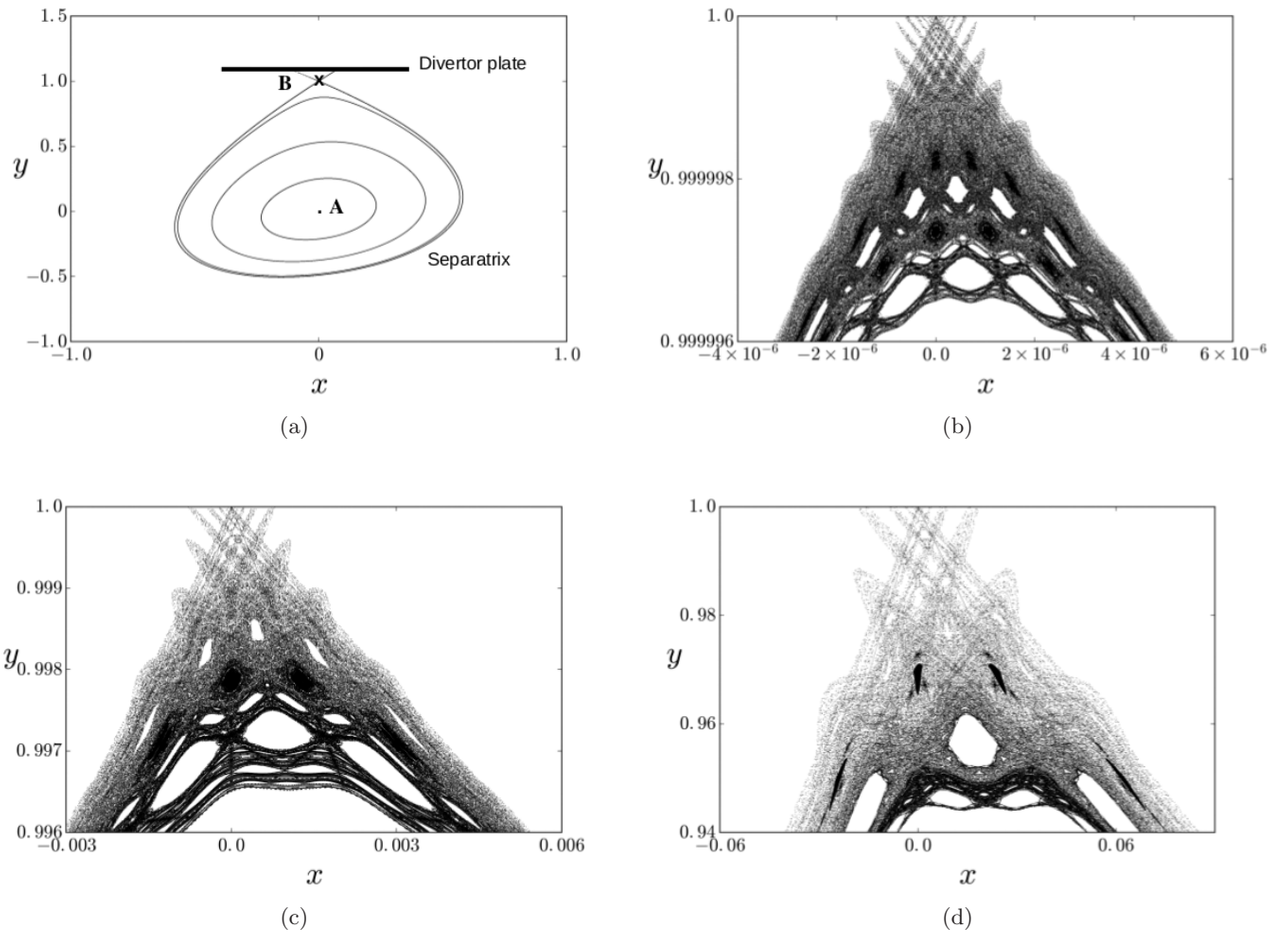

Fig. 2. (a) Phase space of the field line map (10) and (11) for $k = 0.4$. We indicate in the figure the separatrix and the divertor plate positions. Enlarged view of the chaotic region near the saddle point for (b) $k = 0.4$, (c) $k = 0.6$ and (d) $k = 0.8$.

magnetic perturbations created by error fields due to asymmetries on the external coils [Pomphrey & Reiman, 1992].

This nonintegrable element has been introduced in a field line map of the form (10) and (11) by Punjabi *et al.* [1992]

$$x_{n+1} = x_n - k y_n(1 - y_n), \tag{10}$$

$$y_{n+1} = y_n + k x_{n+1}, \tag{11}$$

where $k > 0$ is a tunable parameter which quantifies the nonintegrable effect necessary to create chaotic field lines. (x_n, y_n) are the rectangular coordinates of the nth intersection of a given magnetic field line on the poloidal surface section, Fig. 1(b). Its Jacobian matrix

$$\mathbf{J} = \begin{pmatrix} 1 & k(2y_n - 1) \\ k & 1 + k^2(2y_n - 1) \end{pmatrix} \tag{12}$$

satisfies the area-preservation condition (7) for all values of k.

The map (10) and (11) has two fixed points: $\mathbf{A} = (0, 0)$ and $\mathbf{B} = (0, 1)$. From (12) $\mathbf{A}$ is stable (a center elliptic point) provided $0 < k < 2$, whereas $\mathbf{B}$ is unstable (a hyperbolic saddle point) in the same interval of k. In physical terms $\mathbf{A}$ corresponds to the magnetic axis, and $\mathbf{B}$ is the intersection between the separatrix and the y-axis.

By linearizing the map (10)–(11) around the center $\mathbf{A}$, the safety factor q_{axis} in this neighborhood is given by

$$\sin\left(\frac{2\pi}{q_{\text{axis}}}\right) = k\sqrt{1 - \frac{k^2}{4}}. \tag{13}$$

For example, if $k = 0.6$ the safety factor close to the magnetic axis will be $q_{\text{axis}} \approx 10$, which is a value too large as compared with experiments. In order to provide a more realistic value we will introduce a parameter N_ϕ, which is the number of map iterations equivalent to one toroidal turn along the ϕ-direction. In other models, it is customary to have $N_\phi = 1$. This parameter is introduced to have a realistic profile of the safety factor. Accordingly, for $k = 0.6$ we get $q_{\text{axis}} \approx 10$ and $q_{\text{edge}} \approx 30$, so that $N_\phi = 10$ renders $q_{\text{axis}} \approx 10$ and $q_{\text{edge}} \approx 30$ [Horton, 2018]. This means that each iteration corresponds to a toroidal advance of $\Delta\phi = 2\pi/N_\phi = \pi/5$.

For any nonzero value of k, the system is nonintegrable and chaotic field lines are possible. We use the word chaos in the Lagrangian sense: two initially close field lines become exponentially separated after a number of toroidal turns along the tokamak. Actually the toroidal angle plays the role of time, since the magnetic field is considered to be strictly time-independent.

On the other hand, more sophisticated maps were proposed by Abdullaev *et al.* to investigate the line trajectories near the hyperbolic saddle point in tokamaks with divertors [Abdullaev & Zaslavsky, 1995, 1996; Abdullaev *et al.*, 1998; Abdullaev & Finken, 1998]. These maps, while quite accurate, involve intricate integrals disturbing terms, making their applicability too elaborate. This greatly diminishes the advantage of explicit maps, compared to numerical integrations of the differential equations of field lines, to study the influence of real asymmetric magnetic perturbations on the field lines and the pattern of magnetic footprints on the divertor plates.

The phase space for the map (10) and (11) is shown in Fig. 2(a) for $k = 0.4$, where we can identify the fixed points $\mathbf{A}$ and $\mathbf{B}$ and a number of closed orbits corresponding to magnetic surfaces responsible for the plasma confinement. We also show a separatrix connecting the invariant manifold originating from the saddle point $\mathbf{B}$. The homoclinic orbit corresponds to the plasma boundary and the two outward branches of these manifolds intercept the divertor plate, which is placed just after $y = 1.0$. The chaotic region near the separatrix is best observed in the magnification in the vicinity of $\mathbf{B}$ [Fig. 2(b)]. This area-filling region becomes more pronounced as k increases from 0.6 [Fig. 2(c)] to 0.8 [Fig. 2(d)].

The smaller k is, the closer the last magnetic surface is to point $\mathbf{B}$. It is also possible to observe magnetic islands immersed in the chaotic layer, which are known to produce stickiness of the field lines around the last chain of islands due to the high concentration of points in these locations, influencing field line escape [Kroetz *et al.*, 2008].

The origin of the chaotic magnetic field line layer is the homoclinic tangle formed by intersections of the stable and unstable manifolds of the saddle point $\mathbf{B}$, their internal branches being shown in Figs. 3(a) and 3(b), respectively, for $k = 0.6$ [da Silva *et al.*, 2002]. We obtained the unstable and stable manifolds from evolving forwards and backwards, respectively, a small disk filled with initial conditions and centered at an unstable periodic orbit embedded in the chaotic layer. The external

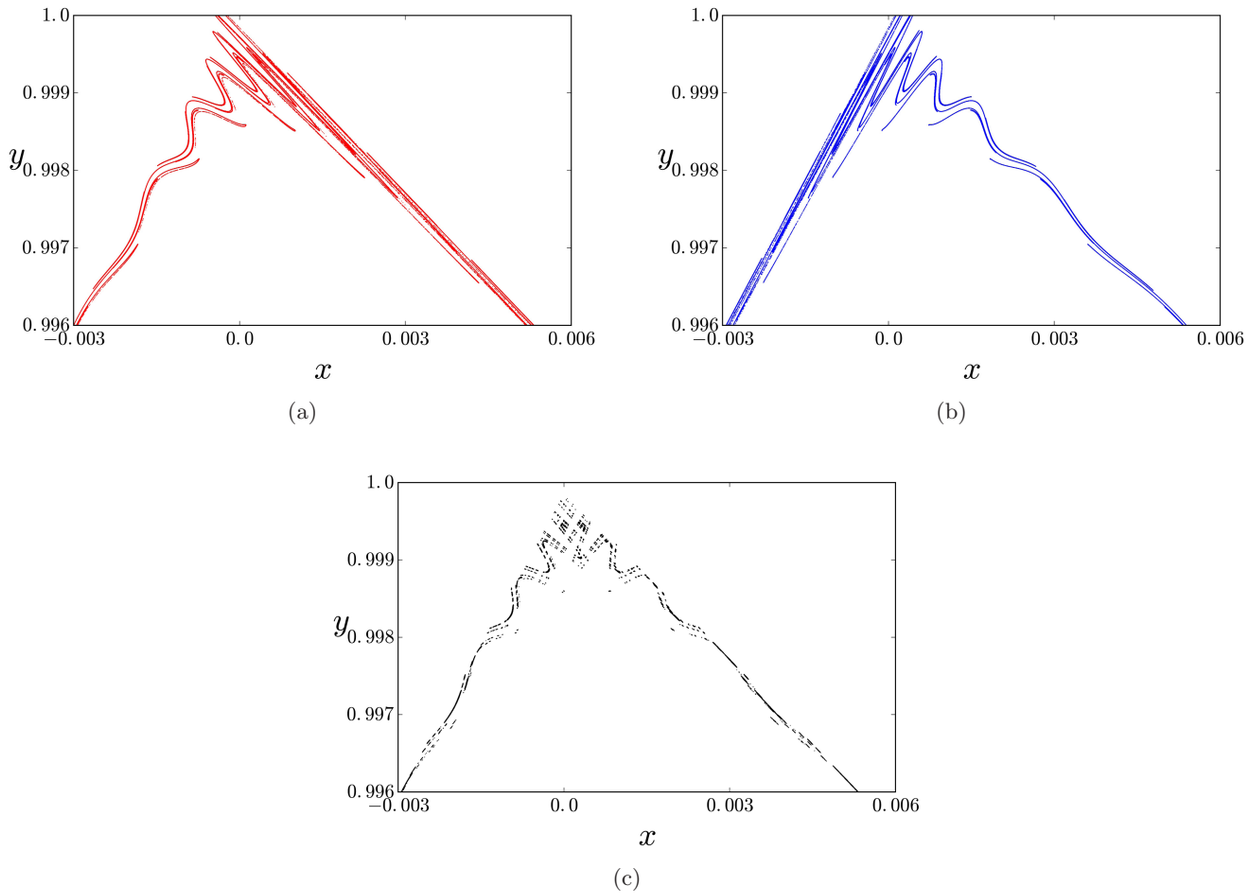

Fig. 3. (a) Stable and (b) unstable manifold and (c) chaotic saddle for a chaotic orbit of the map (10) and (11) for $k = 0.6$.

branches of these manifolds are similar except that they eventually reach the divertor plate.

The intersections of the stable and unstable manifolds form an invariant nonattracting chaotic set called *chaotic saddle* [Péntek *et al.*, 1995]. A numerical approximation of it is depicted in Fig. 3(c). Topologically, the chaotic saddle is similar to a Cantor dust with zero Lebesgue measure: if we randomly choose a field line in the chaotic region, the probability of this line being exactly on the saddle is zero. Notwithstanding, a field line off but very close to the chaotic saddle will wander through the chaotic region approximately following the unstable manifold until being diverted to the plate.

4. Magnetic Footprints

4.1. *Continuous description of magnetic field lines*

The magnetic footprints are defined as sets of points where the field lines strike the divertor plate. We have seen that the invariant manifolds stemming from the unstable periodic orbits embedded in the chaotic saddle act as escape channels for field lines. Hence we expect that the magnetic footprints are projections of the invariant manifold structure in the chaotic field line region.

The description of field lines from a discrete mapping would give us only a one-dimensional projection of the magnetic footprints on the divertor plate, preventing us from obtaining an accurate determination of the strike points. Moreover the divertor plate is extended along the toroidal direction, and thus the mapping procedure has to be modified in order to provide a proper visualization of magnetic footprints. Accordingly, we transform the timelike variable from a discrete n to a continuous parameter φ defined as

$$\varphi = \frac{N_\phi}{2\pi}\,\phi, \tag{14}$$

in such a way that φ is proportional to the toroidal angle ϕ and acts as a interpolating parameter

allowing us to determine the strike point at which a field line intercepts the divertor plate. Thus, the introduction of a continuous time variable give us a two-dimensional footprints view, comparable to those observed in experiments.

We thus modify the map (10) and (11) to include this continuous parameter:

$$x(\varphi) = x_n - k\varphi y_n(1 - y_n), \tag{15}$$

$$y(\varphi) = y_n + k\varphi x(\varphi), \tag{16}$$

where $0 \leq \varphi \leq 1$ acts as an interpolating parameter between two iterations of the map, such that

$$(x(0), y(0)) = (x_n, y_n), \tag{17}$$

$$(x(1), y(1)) = (x_{n+1}, y_{n+1}). \tag{18}$$

Another advantage of using the continuous variable φ is that it can be used as a timelike variable in a Hamiltonian description of field line dynamics. In this case (x, y) are respectively the coordinate and canonically conjugated momentum, with the corresponding Hamilton equations

$$\frac{dx}{d\varphi} = \frac{\partial H}{\partial y}, \tag{19}$$

$$\frac{dy}{d\varphi} = -\frac{\partial H}{\partial x}, \tag{20}$$

where φ is the canonical time and H is the field line Hamiltonian. In this framework, we can regard the map (10) and (11) has solutions similar to those of the canonical equations with the Hamiltonian

$$H(x, y) = \frac{1}{2}k(x^2 + y^2) - \frac{1}{3}ky^3. \tag{21}$$

The Hamiltonian (21) has a mechanical analogous which is a particle subjected to a one-dimensional potential function $U(y) \propto y^2/2 - y^3/3$, such that $U(y \to \pm\infty) \to \mp\infty$. The latter corresponds to a potential well around the center at $(x = 0, y = 0)$ and a hill at the saddle point $(x = 0, y = 1)$. These elliptic and hyberpolic points correspond qualitatively to those generated by the map given by (10) and (11).

Since this Hamiltonian does not depend explicitly on the timelike variable φ the system is integrable and thus cannot describe completely the field line dynamics exhibited by the map (10) and (11). In order to make the system nonintegrable, such that it can present a chaotic orbit, it would be necessary to add a "time"-dependent perturbation to (21).

4.2. *Numerical determination of magnetic footprints*

Given the continuous description previously introduced, it is straightforward to obtain magnetic footprints from Eqs. (15) and (16). Once we set the divertor plate position y_p, we start from an initial condition (x_0, y_0) randomly chosen inside the chaotic layer existent in phase space for any nonzero value of the parameter k. We divide the phase space region in a grid of $10^3 \times 10^3$ initial conditions and iterate the discrete map (10) and (11) for each of these initial conditions by a maximum of 10^4 times or until we reach the divertor plate, i.e. until the condition

$$y_n \leq y_p \leq y_{n+1} \tag{22}$$

is fulfilled. We consider the maximum integration time to be 10^4, in order to obtain as much information as possible from the system. Actually the location, size and shape of the plate can be accommodated in the method. For the results presented here, we choose $y_p = 1.0$.

Once the condition (22) is fulfilled, we look for the coordinates (x_p, y_p) of the strike point, i.e. the point where the field line collides with the divertor plate. The value of φ corresponding to the strike point (denoted by φ_s) is given by (16) as the solution of the following equation

$$y_p = y_n + k\varphi_s[x_n - k\varphi_s y_n(1 - y_n)], \tag{23}$$

and, inserting back the value of φ_s in (15) gives the other coordinate of the strike point

$$x_p = x(\varphi_s) = x_n - k\varphi_s y_n(1 - y_n). \tag{24}$$

The range of φ is limited to two consecutive iterations of the map. If we chose $N_\phi = 10$, from (14) we have that $\Delta\varphi = 1$ corresponds to an angular interval of $\Delta\phi = \pi/5$.

The magnetic footprints obtained by this procedure are shown in Fig. 4 (left panels, where the right panels are magnifications), for $y_p \gtrsim 1.0$ and different values of the parameter k. We show the x-coordinates of the strike points and the corresponding values of φ_s in the interval $[0, 1]$, which corresponds to an angular extension of $\Delta\phi = \pi/5$ of the divertor plate. In a colorscale we also indicate the connection length for each strike point, which is the number of map iterations needed for a given field line to strike the divertor plate.

For $k = 0.4$ the magnetic footprint consists of a set of thin stripes [Fig. 4(a)] with an internal

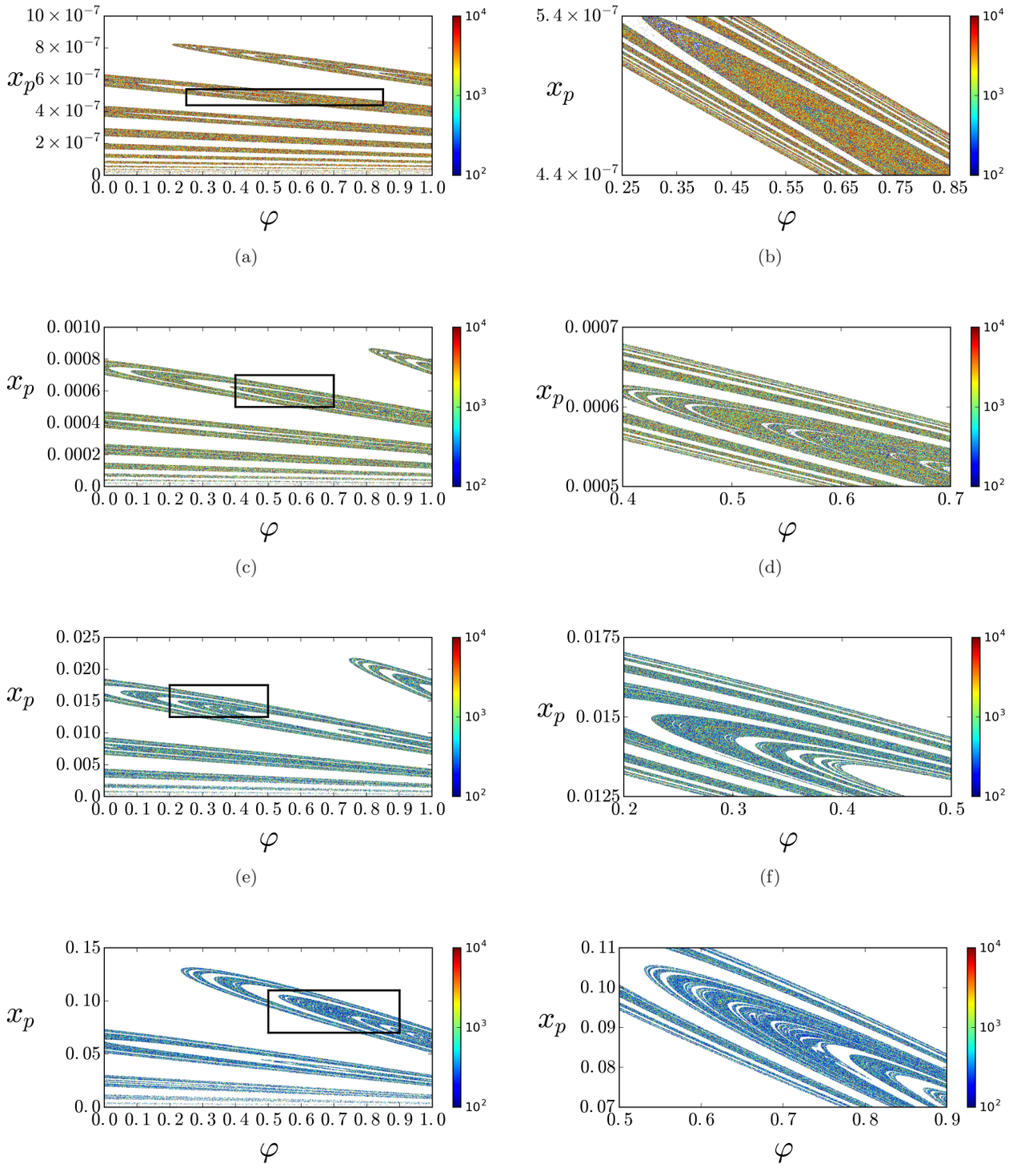

Fig. 4. Magnetic footprints of field lines on the divertor plate ($y_p \gtrsim 1.0$) for $k =$ (a) 0.4, (c) 0.6, (e) 0.8, (g) 1.0, and (i) $k = 1.2$. (b), (d), (f), (h), and (j) are magnifications of the rectangular boxes in (a), (c), (e), (g), and (i), respectively. The colorbar indicates the connection length of each field line striking the divertor plate.

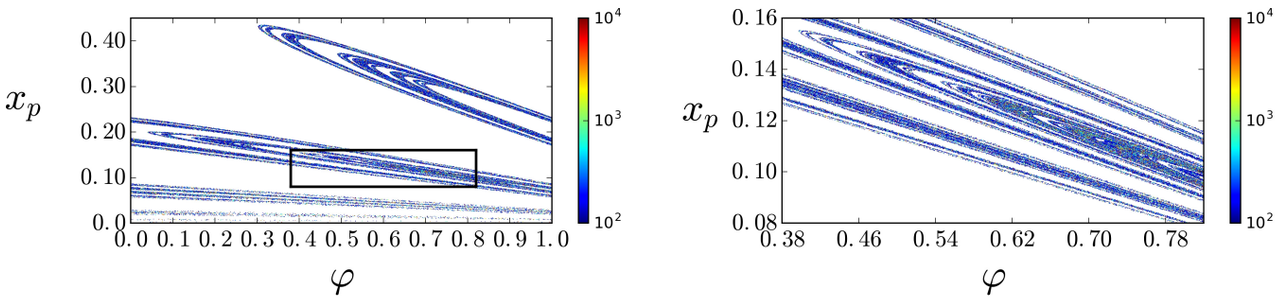

(i) (j)

Fig. 4. (*Continued*)

structure which reminds us of "Saturn rings" [Fig. 4(b)]. The extension of the magnetic footprint is of the order of 10^{-6}, which is compatible with the width of the stochastic layer we see in the corresponding phase space [see Fig. 2(b)]. Most of the strike points have connection lengths higher than 10^3. Those strike points with the higher connection lengths have x_p coordinates close to zero, which is explained by Fig. 4 noting that the density of points therein is higher than for other values of k.

If k is increased to other values [Figs. 4(c)–4(j)] we see a repetition of this pattern of thin stripes with a self-similar structure. The size of the magnetic footprint is seen to increase with k, that follows from the increase of the width w of the chaotic layer near the separatrix [Punjabi *et al.*, 1996]. The chaotic layer can be approximated by an annulus of inner radius 1 and outer radius $1 - w$, the latter being the outermost closed orbit, which also marks the plasma boundary, since it is the intersection of the last intact magnetic surface with the Poincaré surface section.

For higher values of k we also observe more often the presence of field lines with low connection lengths ($\sim 10^2$). This has important consequences in terms of the distribution of heat loads on the divertor plate. Assuming that plasma particles closely follow field lines (with a small Larmor radius) it follows that magnetic field lines with large connection lengths can come from inner regions of the chaotic layer (regions closer to the magnetic axis), so close to the plasma boundary that they can bring energetic particles from the plasma core to the divertor plate. These particles are responsible for a high degree of heat load, which may result in the liberation of impurities from the metallic plate through sputtering processes and other plasma-wall interaction phenomena.

Given the chaotic nature of the field lines striking the divertor plate, one could erroneously assume that the heat loads could be distributed uniformly. The self-similar structure of the magnetic footprints, however, shows that this is not so, and hot spots with large heat loads are possible due to the dynamics underlying the chaotic orbit. However, the fractal nature of the dynamics is expected, since the structure of invariant manifolds cross themselves in an infinite number of homoclinic and heteroclinic points close to a saddle point [Péntek *et al.*, 1995].

5. Characterization of Magnetic Footprints

In this work, we are interested in showing that the magnetic footprints of divertor map (Fig. 4) are fractals. Accordingly, we analyze the fractal nature of the structure in the magnetic footprints by computing the so-called basin entropy to quantify the degree of uncertainty due to the fractality of the basin and of the basin boundary [Daza *et al.*, 2016, 2017]. We define the basin as the set formed by the points of the magnetic footprints.

5.1. *Basin entropy*

An alternative measure of the unpredictability is to apply the proposed method for the calculation of basin entropies. This method quantifies the degree of uncertainty due to the fractality of basin of the magnetic footprint. We consider two basins: the white basin of the magnetic footprints formed by set of points where the field lines are striking the divertor plate with low connection lengths (between 1–100 iterations) and the colored basin of the magnetic footprints formed by set of points where the

field lines strike the divertor plate with connection lengths between 101–10000 iterations. The basic idea of the technique is to divide the phase space in N boxes of linear size ε, each of them containing a number N_c of initial conditions which evolve through time towards a given basin (white or colored points), so that we will refer to that application as a color. Let a positive integer i denote a box ($i = 1, 2, \ldots, N$) and j a possible basin ($j = 1, 2, \ldots, N_A$). For the ith box, the fraction of initial conditions resulting in jth basin defines a probability $p_{i,j}$, such that the entropy of each box is:

$$S_i = \sum_{j=1}^{N_A} p_{i,j} \ln\left(\frac{1}{p_{i,j}}\right). \tag{25}$$

In our case there are only $N_A = 2$ basins (white or colored points) inside the ith box. The total entropy for the phase space is obtained by the addition of the entropy associated to each one of the N boxes: $S = \sum_{i=1}^{N} S_i$. This entropy can be computed for any given basin, such that the basin entropy is the total entropy divided by the number of boxes: $S_b = S/N$. The basin entropy quantifies the degree of uncertainty of the basin, that is, for a single basin, the basin entropy is zero, meaning zero uncertainty, whereas for N_A equiprobable basins $S_b = \ln N_A$, which means a completely randomised basin structure.

As we are also interested in the uncertainty of the boundary, in particular, we want to know if the critical boundary (Fig. 4) is fractal, we restrict the calculation of the basin entropy to the boxes in the vicinity of the boundaries. For this, we compute the entropy only for those boxes N_b which contain the two cases (white and colored points): $S_{bb} = S/N_b$. Therefore, the quantity S_{bb} is the so-called basin boundary entropy that measures the complexity of the basin boundary. Moreover, there is a threshold value of S_{bb} that separates basins with smooth boundaries from those with fractal boundaries. For example, suppose that our basins were separated by a smooth boundary, the number of boxes in the boundary will be negligible for the computation of the basin entropy in the boundary S_{bb}, since there are many more boxes with just one basin. Thus, the maximum possible value of S_{bb} that a smooth boundary can have is $\ln 2$. Therefore, if $S_{bb} > \ln 2$, the basin boundary is said to be fractal. This is a sufficient but not necessary criterion for fractality, though, since some fractal basins do not fulfill this condition [Mathias *et al.*, 2017a, 2017b; Mugnaine *et al.*, 2018]. For the criterion $S_{bb} > \ln 2$ to be valid the system must have more than two basins.

Applying those concepts to magnetic footprints, let us compute the basin entropy and the basin boundary entropy. We compute the standard deviation of the basin entropies in the following way: We vary the grid of phase space considering 250×250, 200×200, 125×125 and 100×100 boxes, with 16, 25, 64, 100 points per box, respectively. In each box we calculate the probabilities of obtaining the number of points corresponding to the white and colored basins of the phase space.

Our results for both basin entropy and basin boundary entropy are summarised in Table 1 for the values of parameters $k = 0.4$, $k = 0.6$, $k = 0.8$, $k = 1.0$ and $k = 1.2$. As a trend, the basin entropy increases as the parameter k reaches the value 1.0 and then decreases at $k = 1.2$. The same happens with the basin boundary entropy, S_{bb} increases as the parameter k reaches the value 1.0 and then decreases at $k = 1.2$. From that, we can say that the white and colored basin boundaries of Fig. 4 are more mixed and involved for the value of parameters $k = 0.8$ and $k = 1.0$, since both have the same values with the standard deviation.

The behavior of the entropies can be qualitatively understood by comparing them with the fraction occupied by the basin $\mathcal{A}$, which corresponds

Table 1. Basin entropy S_b, basin boundary entropy S_{bb} and fraction occupied by the colored basin of magnetic footprint $\mathcal{A}$ for the values of parameters $k = 0.4$, $k = 0.6$, $k = 0.8$, $k = 1.0$ and $k = 1.2$. $\overline{n}$ is the average escape time of each magnetic footprint, respectively.

k	0.4	0.6	0.8	1.0	1.2
S_b	0.562 ± 0.056	0.564 ± 0.055	0.613 ± 0.055	0.627 ± 0.055	0.372 ± 0.005
S_{bb}	0.594 ± 0.012	0.595 ± 0.011	0.650 ± 0.002	0.647 ± 0.018	0.445 ± 0.072
$\mathcal{A}$	0.70	0.70	0.58	0.43	0.15
$\overline{n}$	2166	1575	898	491	166

to the set of colored points of magnetic footprints. We computed $\mathcal{A}$ for the values of parameters $k = 0.4$, $k = 0.6$, $k = 0.8$, $k = 1.0$ and $k = 1.2$, the results are shown in Table 1. The basin entropy S_b and the basin boundary entropy S_{bb} follow the variation of the fraction occupied by the basin of magnetic footprints. Since the basin entropies measure the degree of mixing of both basins, it follows that the entropies increase as the colored basin becomes of comparable size to the white basin.That is, the maximum entropy value of the basin occurs for $k = 0.8$ and $k = 1.0$ when the fraction of the colored basin is approximately 58% and 43% of the total area, respectively. On the other hand, the minimum value of the basin entropy (for $k = 1.2$) has the minimum value of the fraction of the colored basin, roughly 15%. Hence, the degree of complexity of the basin structure varies according to the increasing complexity of the basins, that is, when they become progressively more mixed and involved.

6. Wada Basin Boundaries

The study of Wada basin boundaries in our system has important physical consequences, since the information obtained on the plate of divertor is highly complex. The results show that points (field lines) very close together take longer to reach the plate of divertor than others, making it impossible to predict the region of the chaotic layer to which the field line belongs.

In order to look for Wada property in our system we analyze the escape time or number of toroidal turns that each field line makes before reaching the plate and we classify the results in three situations: fast escape, medium escape and slow escape. Let A be the fast escape basin, it has a boundary point p if each neighbor of p intersects basin A and at least one other basin, like B (medium escape basin) or C (slow escape basin). The boundary point p is also a point of Wada if each neighbor of p intercepts the three different basins. A basin boundary is said to have the property of Wada if each boundary point of A is a Wada point, such that the boundary of a basin is a boundary of the Wada basin [Nusse & Yorke, 1996].

In Fig. 5, we plot the magnetic footprints considering three intervals of the escape time, fast escape basin A (1–100 iterations), medium escape basin B (101–5000 iterations) and slow escape basin C (5001–10000 iterations). We choose this interval of the escape time in order for better visualization of the Wada property. We associate a color for each interval, white for the basin A, red for the basin B and green for the basin C. The fraction occupied by escape time basins are summarised in Table 2 for the values of parameters $k = 0.4$, $k = 0.6$, $k = 0.8$, $k = 1.0$ and $k = 1.2$. In order to check for the validity of Wada property we exhibit a magnification of a portion of the basins structure, depicted as a rectangular box in Figs. 5(a), 5(c), 5(e), 5(g) and 5(i). The magnifications confirm the presence of strips of the three basins in finer scales, suggesting that at least some of the boundary points have the Wada property, since a small neighborhood of such point will intersect all basins. The Wada property is not fully present in the escape time basin, since there are regions belonging to only a single basin. It is clearly seen in Fig. 5, where certain regions have only a single color. Thus, the boundary is fractal only at the regions that they tend asymptotically to the edge of the basins.

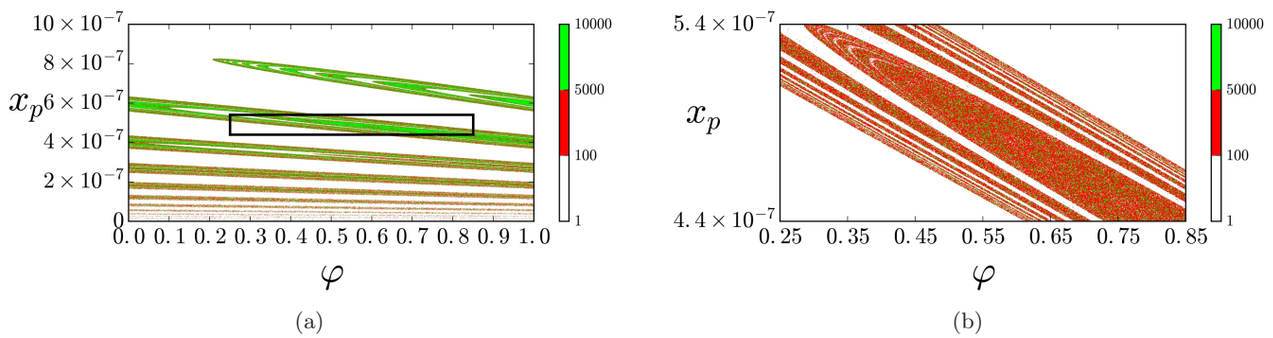

(a) (b)

Fig. 5. Magnetic footprints of field lines on the divertor plate ($y_p \gtrsim 1.0$) for $k =$ (a) 0.4, (c) 0.6, (e) 0.8, (g) 1.0, and (i) $k = 1.2$. (b), (d), (f), (h), and (j) are magnifications of the rectangular boxes in (a), (c), (e), (g), and (i), respectively. The colorbar indicates the connection length of each field line striking the divertor plate, white for the fast escape basin A, red for the medium escape basin B and green for the slow escape basin C.

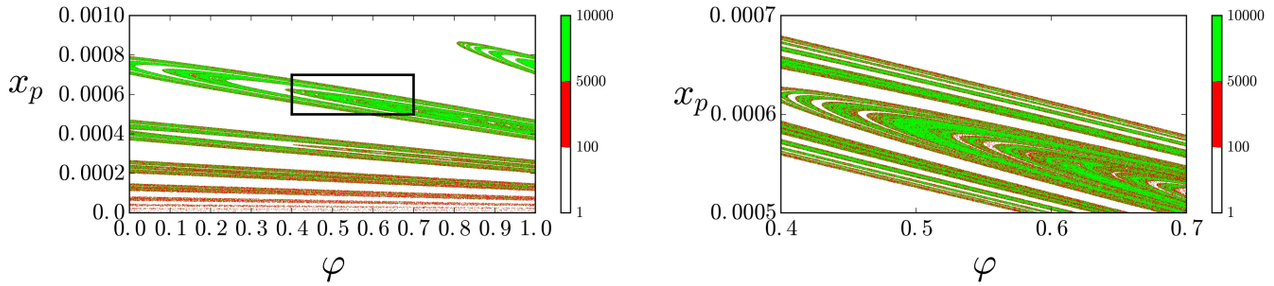

(c)

(d)

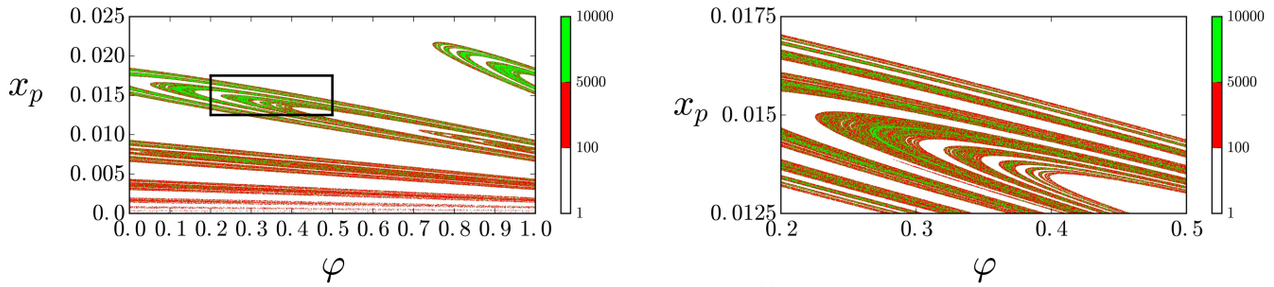

(e)

(f)

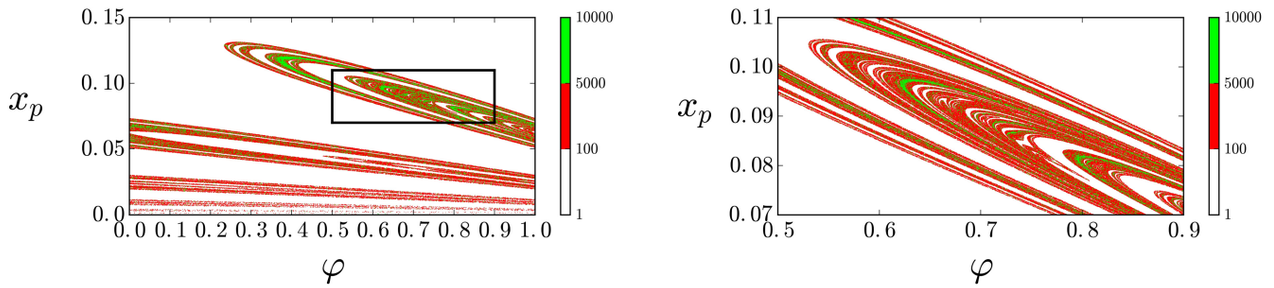

(g)

(h)

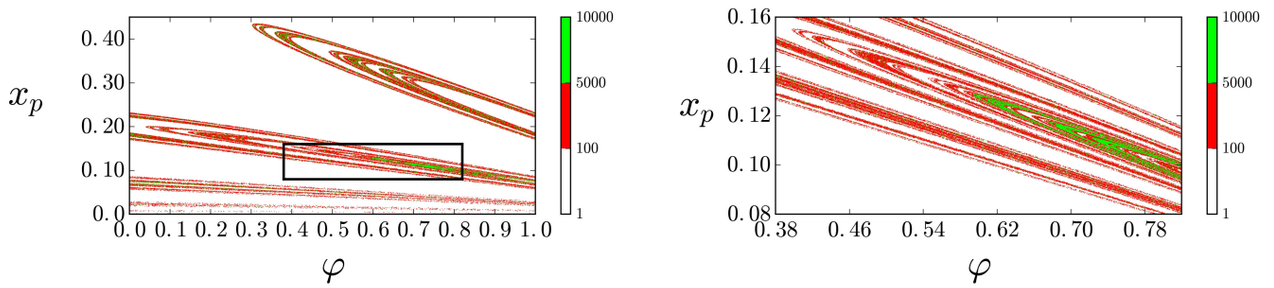

(i)

(j)

Fig. 5. (*Continued*)

Table 2. Fraction occupied by the escape time basins, fast escape A, medium escape B and slow escape C for the values of parameters $k = 0.4$, $k = 0.6$, $k = 0.8$, $k = 1.0$ and $k = 1.2$.

k	0.4	0.6	0.8	1.0	1.2
A	0.30	0.29	0.42	0.57	0.85
B	0.53	0.61	0.54	0.41	0.14
C	0.17	0.10	0.04	0.02	0.01

7. Conclusions

Divertors in tokamaks are devices designed to control magnetic field lines, creating specific escape channels for plasma particles. The deposition patterns of escaping particles onto the divertors plate are called the magnetic footprints. Due to chaotic field lines, magnetic footprints typically exhibit a fractal structure, which has a noneven distribution pattern.

To model such a phenomenon we have used the simple map by Punjabi *et al.* [1992]. The phase space of the simple map is characterized by the existence of two fixed points, one saddle and another center. The escaping field lines are separated from the confined field lines by a separatrix which is formed by the stable and unstable manifolds of the saddle point.

For the chosen parameters, a chaotic layer and magnetic islands emerge near the separatrix. We have numerically calculated the stable and unstable manifolds of the chaotic saddle for this scenario and showed how they delineate the escape channels to the divertors plate.

To further evaluate the magnetic footprints, we used the basin entropy to quantify the basin structure of the magnetic footprints. This is a more direct measure to compute the loss of information on the final state of the system. The basin boundary entropy varies between zero (in the case of just one final state, meaning no uncertainty at all) and unity (for two possible final state), when the basins are extremely intertwined and we have maximum final-state uncertainty.

We found that both the basin and basin boundary entropies depend on the control parameter in the same way as the fraction of phase space occupied by the basin of magnetic footprints. The basin entropy increases as the parameter k reaches the value 1.0 and then decreases at $k = 1.2$. Since the basin entropies measure the degree of mixing of the basins, it follows that the basin entropies increase as the colored basin becomes of comparable size to the white basin, i.e. for $k = 0.8$ and $k = 1.0$ the fraction of the colored basin is roughly 58% and 43%, respectively. However, the basin boundary entropy has maximum value at for $k = 0.8$ and $k = 1.0$, since the basins boundaries have a more interwined structure.

Another fractal signature we found in escape time basin is the Wada property. We verify in our system, through magnifications of the magnetic footprints the presence of strips of the three basins in finer scales, revealing a part of the third basin where it seemed to be the boundary between the two other basins.

In this work we showed the fractal deposition pattern of magnetic field lines on the divertor plate caused by magnetic perturbations. For values lower than the perturbation parameter ($k = 0.4$ and $k = 0.6$), the fractal distribution of the field lines over the divertor plate resulted in regions with high particle density and energy. However, when the perturbation reaches the value of $k = 1.2$, the deposition pattern of the field lines on the plate is more uniform, that is, the particles are more distributed over the plate and less energetic.

Acknowledgments

This work has been supported by grants from the Brazilian Government Agencies CNPq (proc. 301019/2019-3) CAPES (proc. 88887.320059/2019-00, 407299/2018-1 and 302665/2017-0) and FAPESP (grant 2018/03211-6).

References

Abdullaev, S. S. & Zaslavsky, G. [1995] "Self-similarity of stochastic magnetic field lines near the x-point," *Phys. Plasmas* **2**, 4533–4541.

Abdullaev, S. S. & Zaslavsky, G. [1996] "Application of the separatrix map to study perturbed magnetic field lines near the separatrix," *Phys. Plasmas* **3**, 516–518.

Abdullaev, S. S. & Finken, K. H. [1998] "Widening the magnetic footprints in a poloidal divertor tokamak: A proposal," *Nuclear Fusion* **4**, 531–545.

Abdullaev, S. S., Finken, K. H. Kaleck, A. & Spatschek, K. H. [1998] "Twist mapping for the dynamics of magnetic field lines in a tokamak ergodic divertor," *Phys. Plasmas* **5**, 196–210.

Abdullaev, S. S., Finken, K. H. & Spatschek, K. H. [1999] "Asymptotical and mapping methods in study of ergodic divertor magnetic field in a toroidal system," *Phys. Plasmas* **6**, 153–174.

Abdullaev, S. S., Eich, T. & Finken, K. H. [2001] "Fractal structure of the magnetic field in the laminar zone

of the dynamic ergodic divertor of the torus experiment for technology-oriented research (textor-94)," *Phys. Plasmas* **8**, 2739–2749.

Agency, I. A. E. [2002] *ITER Technical Basis*, No. 24 ITER EDA Documentation Series (International Atomic Energy Agency, Vienna).

Aguirre, J., Viana, R. L. & Sanjuán, M. A. F. [2001] "Fractal structures in nonlinear dynamics," *Rev. Mod. Phys.* **81**, 333–386.

Bernardin, M. P. & Tataronis, J. A. [1985] "Hamiltonian approach to the existence of magnetic surfaces," *J. Math. Phys.* **26**, 2370–2380.

Bertolini, E. *et al.* [1992] "The jet divertor coils," *IEEE Trans. Magn.* **28**, 275–278.

Cordey, J. G., Goldsron, R. J. & Parker, R. R. [1992] "Progress toward a tokamak fusion reactor," *Phys. Today* **45**, 22–30.

da Silva, E. C., Caldas, I. L., Viana, R. L. & Sanjuán, M. A. F. [2002] "Escape patterns, magnetic footprints, and homoclinic tangles due to ergodic magnetic limiters," *Phys. Plasmas* **9**, 4917–4928.

Daza, A., Wagemakers, A., Georgeot, B., Guéry-Odelin, D. & Sanjuán, M. A. F. [2016] "Basin entropy: A new tool to analyze uncertainty in dynamical systems," *Sci. Rep.* **6**, 31416.

Daza, A., Wagemakers, A., Georgeot, B., Guéry-Odelin, D. & Sanjuán, M. A. F. [2017] "Chaotic dynamics and fractal structures in experiments with cold atoms," *Phys. Rev. A* **95**, 013629.

Federici, G. *et al.* [2003] "Key iter plasma edge and plasma-material interaction issues," *J. Nucl. Mater.* **313**, 11–22.

Horton, W. [2018] *Turbulent Transport in Magnetized Plasmas*, 2nd edition (World Scientific).

Horton, C. W. & Benkadda, S. [2015] *ITER Physics* (World Scientific, Singapore).

Jakubowski, M. W., Evans, T. E., Fenstermacher, M. E., Groth, M., Lasnier, C. J., Leonard, A. W. *et al.* [2009] "Overview of the results on divertor heat loads in RMP controlled H-mode plasmas on DIII-D," *Nucl. Fusion* **49**, 095013.

Kroetz, T., Roberto, M., da Silva, E. C., Caldas, I. L. & Viana, R. L. [2008] "Escape patterns of chaotic magnetic field lines in a tokamak with reversed magnetic shear and an ergodic limiter," *Phys. Plasmas* **15**, 092310.

Kroetz, T., Roberto, M., Caldas, I. L., Viana, R. L., Morrison, P. J. & Abbamonte, P. [2010] "Integrable maps with non-trivial topology: Application to divertor configurations," *Nucl. Fusion* **50**, 034003.

Lichtenberg, A. & Lieberman, M. [1992] *Regular and Chaotic Dynamics*, 2nd edition (Springer).

Lipschultz, B., LaBombard, B., Terry, J. L., Boswell, C. & Hutchinson, I. H. [2007] "Divertor physics research on alcator c-mod," *Fusion Sci. Technol.* **51**, 369–389.

Mathias, A. C., Kroetz, T., Caldas, I. L. & Viana, R. L. [2017a] "Chaotic magnetic field lines and fractal structures in a tokamak with magnetic limiter," *Chaos Solit. Fract.* **104**, 588–598.

Mathias, A. C., Viana, R. L., Kroetz, T. & Caldas, I. L. [2017b] "Fractal structures in the chaotic motion of charged particles in a magnetized plasma under the influence of drift waves," *Physica A* **469**, 681–694.

Mugnaine, M., Mathias, A. C., Santos, M. S., Batista, A. M., Szezech, J. J. D. & Viana, R. L. [2018] "Dynamical characterization of transport barriers in nontwist Hamiltonian systems," *Phys. Rev. E* **97**, 012214.

Nusse, H. E. & Yorke, J. A. [1996] "Wada basin boundaries and basin cells," *Physica D* **90**, 242–261.

Péntek, A., Toroczkai, Z., Tél, T., Grebogi, C. & Yorke, J. A. [1995] "Fractal boundaries in open hydrodynamical flows: Signatures of chaotic saddles," *Phys. Rev. E* **51**, 4076–4088.

Pomphrey, N. & Reiman, A. [1992] "Effect of nonaxisymmetric perturbations on the structure of a tokamak poloidal divertor," *Phys. Fluids B* **4**, 938–948.

Portela, J. S. E., Caldas, I. L. & Viana, R. L. [2008] "Tokamak magnetic field lines described by simple maps," *Eur. Phys. J. Special Topics* **165**, 195–210.

Post, D. E. & Behrisch, R. [1986] *Introduction to the Physics of Plasma-Wall Interactions in Controlled Fusion* (Plenum Press, NY).

Punjabi, A., Verma, A. & Boozer, A. [1992] "Stochastic broadening of the separatrix of a tokamak divertor," *Phys. Rev. Lett.* **69**, 3322–3325.

Punjabi, A., Verma, A. & Boozer, A. [1996] "The simple map for a single-null divertor tokamak," *J. Plasma Phys.* **56**, 569–603.

Whiteman, K. J. [1977] "Invariants and stability in classical mechanics," *Rep. Prog. Phys.* **40**, 1033–1069.